8

Detection of Optical Radiation in NO_x Optoelectronic Sensors Employing Cavity Enhanced Absorption Spectroscopy

Jacek Wojtas
Military University of Technology
Poland

1. Introduction

Currently there are two main reasons for seeking new methods and technologies that aim to develop new and more perfect sensors detecting various chemical compounds. The first reason is man's striving for an ever better understanding of the surrounding world and the universe. Second, sensors are used to ensure safety, e.g. in the vicinity of factories, in an important objects like airports, in environmental protection, health care, etc. These applications have a significant impact on the performance of sensors. This chapter addresses the issue of some nitrogen oxides (NO_x) sensor designs using some of the most sensitive methods such as cavity enhanced absorption spectroscopy (CEAS) and cavity ring down spectroscopy (CRDS).

Nitrogen oxides are compounds of nitrogen and oxygen. For example, among them very important are nitric oxide (NO), nitrogen dioxide (NO_2) and nitrous oxide (N_2O). According to the HITRAN database, in standard atmosphere[1] their concentration is as follows: NO – about 0.3 ppbv[2], NO_2 – about 0,023 ppbv, N_2O – about 320 ppbv. However, in real ambient air their concentrations are strongly related to meteorological conditions and emission sources (anthropogenic and natural). They are compounds that play a significant role in many different fields. They are important greenhouse gases, and their reactions with H_2O (water) lead to acid rains. For example, nitrous oxide is used as an anaesthetic, especially in dentistry and minor surgery. It produces mild hysteria and laughter. Thus it is also known as 'laughing gas'. Atmospheric photochemistry induces a complicated conversion mechanism between nitrogen oxides [Godish, 2004]. Moreover, NO, NO_2 and N_2O are also characteristic decomposition compounds which are the main products of specific explosives materials. Many of them contain NO_2 groups, which can be detected using spectroscopic detection methods [Moore, 2007].

There are many methods for NO_x detection. For example, in the case of gas chromatography and mass spectrometry, a detection limit of a few dozen ppb is reported

[1] Based on US Standard Atmosphere 1976 from HITRAN database

[2] In the air pollution monitoring, concentration of the substance is often expressed in units of *ppmv* (parts per one million by volume) or *ppbv* (parts per one billion by volume). It specifies the number of molecules of the absorber for all the molecules present in a given volume.

[Shimadzu Scientific Instruments, Drescher & Brown, 2006]. Detection methods using the photoacoustic phenomenon provide a sensitivity of about 20 ppb [Grossel et al., 2007]. In gas detection applications, a special role is played by optoelectronic methods. CRDS and CEAS methods belong to optoelectronic absorption methods, but there are a lot of other optoelectronic methods for the detection of gases and hazardous substances. In Fig. 1 the most popular are shown. All of them have advantages and disadvantages. However, in respect of the specific properties are all widely used. Due to the theme of this chapter the absorption methods will be discussed in more detail.

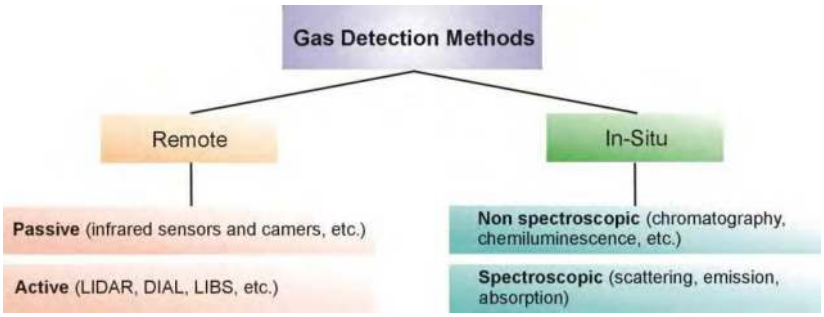

Fig. 1. Popular gas detection methods

In passive methods, an optical radiation emitted by a thermal object is registered. These systems are widely used in infrared cameras and infrared sensors. Such a solution does not require often very costly, radiation sources.
Active methods are more frequently used in remote (standoff) gas detection application. The most commonly are LIDAR's (LIght Detection And Ranging). Typical LIDAR consists of a transmitter that emits laser pulses and an optical radiation receiver. Laser pulses after being scattered in the clouds, aerosols or dust are registered with a photoreceiver. Next, the signal is processed in a digital processing unit. Such a system is used to monitor rainfall, clouds and smoke emerging from chimneys or for the detection of gaseous pollutants of the atmosphere [Mierczyk et al., 2008, Karasinski et al., 2007]. DIAL (Differential Absorption LIDAR) is based on laser radiation measurement at a peak of absorption and at a trough. Thus, a differential signal is received, which is used to determine concentration profiles and mass emissions of various species [Chudzynski et al., 1999]. Laser-induced breakdown spectroscopy (LIBS) uses a highly energetic laser pulses as the excitation source to form plasma, which atomizes and excites samples. The emission from the plasma plume is registered and analyzed with the detection system [Owsik & Janucki, 2004].
The group of examination methods that are used exactly in the place of occurring gas (in-situ) includes non-spectroscopic and spectroscopic methods. These are widely used chemical methods, which belong to the former. They are based on the use of certain chemical reactions, which may indicate the presence of the substance sought [Sigrist, 1994]. The latter are very popular. They can be divided into scattering, emission and absorption methods. In the first, radiation scattered with the sample is examined [Li et al., 2005]. In the second, a probing radiation beam causes the sample excitation. Next, the detection system registers and analyzes the spectrum emitted with the sample. In the third type of spectroscopic method, the absorbed radiation is analyzed. In all spectroscopic methods the properties of the sample are determined on the basis of the measured spectral characteristics of radiation [Lagalante, 1999].

Absorption spectra can be defined as the set of all electron crossings from lower energy levels to higher ones. They cause an increase in molecules energy. In case of the emission spectra there is inverse situation. The spectra correspond to the reduction of molecules energy as a result of electrons transitions from higher energy levels to lower ones. Scattering spectra rely on a change in the frequency spectra diffuse radiation in relation to the frequency of incident radiation, due to the partial change of the photon energy as a result of impact with the molecules. However, in this case there is no effect of radiation absorption or emission [Saleh & Teich, 2007, Sigrist 1994].

2. Principles of absorption spectroscopy

Each gas molecule has a very characteristic arrangement of electron energy levels (vibrational and rotational). As a result of light absorption, particles go to one of the excited states and then in various ways lose energy. Absorption spectroscopy refers to spectroscopic techniques that measure the absorption of radiation, as a function of wavelength, due to its interaction with a sample. The sample absorbs energy, i.e., photons, from the radiating field. The intensity of the absorption varies as a function of wavelength and this variation is the absorption spectrum [Sigrist, 1994]. Absorption spectroscopy is performed across the electromagnetic spectrum. A source of radiation and very sensitive photoreceiver is used which records radiation passing through the absorber sample. During the last several years absorptions methods for gas detection were significantly developed. The simple setup, which shows the idea of absorption method, is presented in Fig. 2.

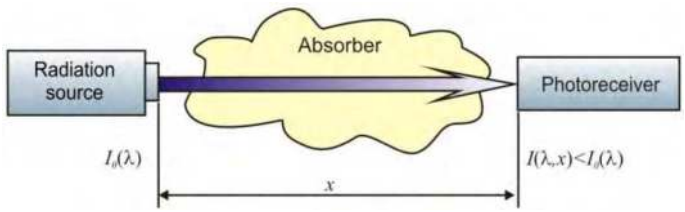

Fig. 2. The absorption method idea.

An arc lamp, LED (Light Emitting Diode) or laser emitting a wavelength matched to the absorption lines of the test gas could be applied as the source of radiation. If an absorber is placed between the source and photoreceiver, the intensity of radiation is weakened. The type and concentration of the test absorber can be inferred on this basis. The intensity of radiation registered with the photoreceiver can be determined using the Lambert-Beer law

$$I(\lambda,x) = I_0(\lambda)\exp(-x\sigma(\lambda)C)\,, \tag{1}$$

where $I_0(\lambda)$ is the intensity of radiation emitted by the source, x is the path of light in the absorber, C - concentration of the investigated gas, while $\sigma(\lambda)$ is the absorption cross section. The cross section is the characteristic parameter of the gas and it can be determined during the laboratory experiment. Knowledge regarding the intensity of radiation emitted from the source, the intensity of received radiation, the absorption cross section and the distance x, provides the possibility of gas concentration calculation from the formula

$$C = \log\left(\frac{I_0(\lambda)}{I(\lambda, x)}\right) \cdot (\sigma(\lambda) \cdot x)^{-1}. \quad (2)$$

One of the most common gas detection systems is differential optical absorption spectroscopy (DOAS). The first system was applied by Ulrich Platt in the 1970's. Currently, similar arrangements are applied to the monitoring of atmospheric pollutants, including the detection of NO_x, in terrestrial applications, in air and in the space, e.g. GOME and SCIAMACHY satellite. Sensitivity of the method depends on the distance between the radiation source and the photoreceiver. For systems where this distance is a few kilometres, the sensitivity of the DOAS method is better than 1 ppb in the case of NO_2 detection [Martin et al., 2004, Wang et al., 2005, Noel et al., 1999].
In order to lengthen the optical path and to improve the sensitivity of absorption methods, reflective multipass cells are used, e.g. in tuneable diode laser absorption spectroscopy (TDLAS). This method is characterized by high sensitivity. Applications cells with lengths of a few dozen meters provide the possibility to achieve a sensitivity of 1 ppb and higher [Jean-Franqois et al., 1999, Horii et al., 1999].
There are many differ concepts applied to gas detection and identification. However, optoelectronic methods enable a direct and selective measurement of concentration on the level of a single ppb.

3. Idea of the CRDS and other cavity enhanced methods

Cavity ring down spectroscopy for the first time was applied to determine the reflectivity mirrors by J.M. Herbelin [Herbelin et al., 1980]. CRDS provides a much higher sensitivity than conventional absorption spectroscopy. The idea of the CRDS method is shown in Fig. 3. In this method there is applied an optical cavity with a high quality factor that is made up of two concave mirrors with very high reflectivity *R*. This results in a long optical path, even up to several kilometres [Busch & Busch, 1999].

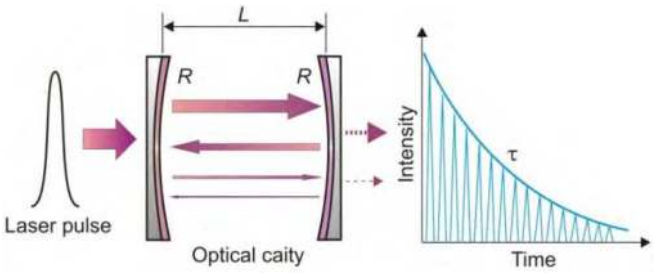

Fig. 3. Cavity ring down spectroscopy idea.

A pulse of optical radiation is injected into the cavity through one of the mirrors. Then inside the cavity multiple reflections occur. After each reflection, part of the radiation exiting from the cavity is registered with the photodetector. The output signal from the photodetector is proportional to the intensity of radiation propagated inside the optical cavity. If the laser wavelength is matched to the absorption spectra of gas filling the cavity, the cavity quality decreases. Thus, parameters of the signal from the photodetector are

changed. Thanks to this, the absorption coefficient and concentration of gas can be determined. The methods of their determination will be discussed in a subsequent section.

3.1 Characteristics of common cavity enhanced systems

Currently there are used many types of cavity enhanced systems that are characterized by different technical constructions and properties. The literature shows that most of them use:

- P-CRDS method (called Pulsed), which uses pulsed lasers [O'Keefe & Deacon, 1988],
- CW-CRDS method (called Continuous Wave) applying continuous operation lasers [He & Orr, 2000],
- CEAS and ICOS (Integrated Cavity Output Spectroscopy) methods basis on off-axis arrangement of the radiation beam and optical cavity [Kasyutich et al., 2003a],
- cavity evanescent ring-down spectroscopy (EW-CRDS), which uses the evanescent wave phenomenon [Pipino, 1999],
- fibber-optic CRDS (F-CRDS) [Atherton et al., 2004],
- ring-down spectral photography (RSP) – a broadband spectroscopy of optical losses [Czyzewski et al., 2001, Stelmaszczyk et al., 2009, Scherer et al., 2001].

The greatest sensitivity of the method is characterized by P-CRDS, CW-CRDS and CEAS [Ye et al., 1997, Berden et al., 2000]. For this reason they are often used for detecting and measuring gas concentrations [Kasyutich et al., 2003b]. The P-CRDS method was first used in 1988 to measure the absorption coefficient of gas [O'Keefe & Deacon, 1988]. Typical schematic layout is shown in Fig. 4.

This method involves the use of a pulsed radiation source, characterized by a broad spectrum of the pulse. This leads to the excitation of multiple longitudinal of the resonance cavity, and also reduces the sensitivity. Sensitivity of the P-CRDS usually reaches values corresponding to the absorption coefficients of the order of 10^{-6} - 19^{-10} cm^{-1} [Busch & Busch, 1999].

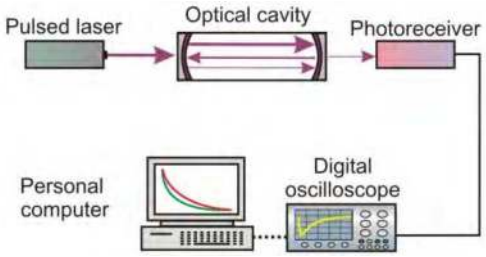

Fig. 4. Diagram of the P-CRDS setup.

CW-CRDS for gas detection has been used since 1997 [Romanini et al., 1997]. A simplified diagram of the experimental setup is shown in Fig. 5. The use of continuous operating lasers in the CRDS technique was possible through the use of different laser beam modulators (e.g. acusto-optic) [Berden et al., 2000]. Due to the narrow spectral lines available with these lasers, operation in a single longitudinal mode is possible in longer optical cavities. Thanks to this CW-CRDS has the highest sensitivity among the cavity enhanced methods. The extreme sensitivity of this method reaches the level of absorption coefficients of up to 10^{-14} cm^{-1}. Due to the high spectral resolution of CW-CRDS, the method is often used in absorption spectra measurements [Busch & Busch, 1999].

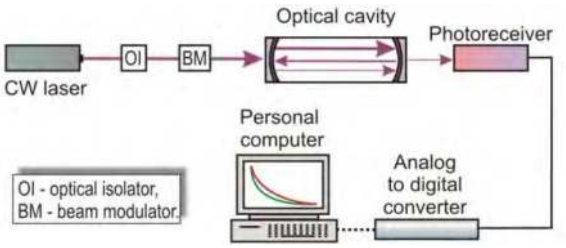

Fig. 5. Experimental CW-CRDS.

The main drawback of this method is the very high sensitivity of the mechanical instability. If the laser frequency is matched to the cavity mode, there is a very efficient storage of light (Fig. 6). However, fluctuations in the frequency of their own cavity, for example due to a change in its length due to mechanical vibrations, cause the optical resonance phenomenon to become impossible and it lead to high volatility of the output signal [Berden et al., 2000].

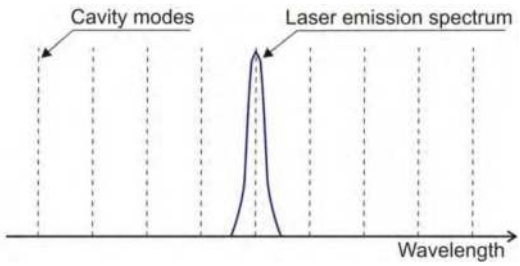

Fig. 6. Coupling of the modes structure of the cavity and cw type laser in the CW-CRDS.

In 1998, R. Engeln proposed a new method – cavity enhanced absorption spectroscopy (also called ICOS), whose principle of operation is very similar to CRDS. The main difference relates to a laser and the optical cavity alignment [Engeln et al., 1998]. In this technique the laser beam is injected at a very small angle in respect to the cavity axis (Fig. 7). As the result, a dense structure of weak modes is obtained or the modes do not occur due to overlapping. Sometimes, in addition to the output mirror, a piezoelectric-driven mount that modulates the cavity length is used in order to prevent the establishment of a constant mode structure within the cavity [Paul et al., 2001]. The weak mode structure causes that the entire system is much less sensitive to instability in the cavity and to instability in laser frequencies. Additionally, due to off-axis illumination of the front mirror, the source interference by the optical feedback from the cavity is eliminated. CEAS sensors attain a detection limit of about 10^{-9} cm^{-1} [Berden et al., 2000, Courtillot et al., 2006]. Therefore, this method creates the best opportunity to develop a portable optoelectronic sensor of nitrogen oxides.

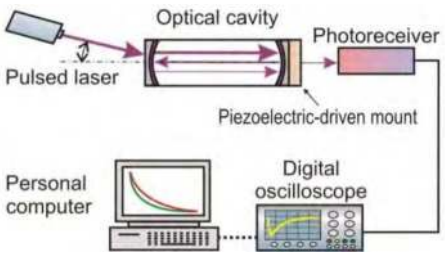

Fig. 7. The scheme of CEAS setup.

3.2 Methods for gas concentration determination used in cavity enhanced spectroscopy

In the methods described in the previous section, several methods are used to determine the gas concentration: by measuring the decay time of the signal, by measuring the phase shift and by measuring the signal amplitude [Busch & Busch, 1999, Berden et al., 2000, Wojtas et al., 2005].

If the laser pulse duration is negligibly short and only the main transverse mode of the cavity is excited, then exponential decay of radiation intensity can be observed

$$I(t) = I_0 \exp\left(-\frac{t}{\tau}\right). \tag{3}$$

If intrinsic cavity losses can be disregarded, the decay time of signal in the cavity (τ) depends on the reflectivity of mirrors R, diffraction losses and the extinction coefficient a, i.e. the scattering and absorption of radiation occurring in the gas filling the cavity

$$\tau = \frac{L}{c(1 - R + \alpha L)}, \tag{4}$$

where L is the length of the resonator, c - speed of light. Determination of the concentration of the examined gas is a two-step process. First, measurement of the signal decay time (τ_0) in the optical cavity not containing the absorber (tested gas) is performed (Fig. 8-A), and then measuring the signal decay time τ in the cavity filled with the tested gas is carried out (Fig. 8-B). Knowing the absorption cross section (σ) of the examined gas, its concentration can be calculated from the formula

$$C = \frac{1}{c\sigma}\left(\frac{1}{\tau} - \frac{1}{\tau_0}\right), \tag{5}$$

where

$$\tau_0 = \frac{L}{c(1 - R)}. \tag{6}$$

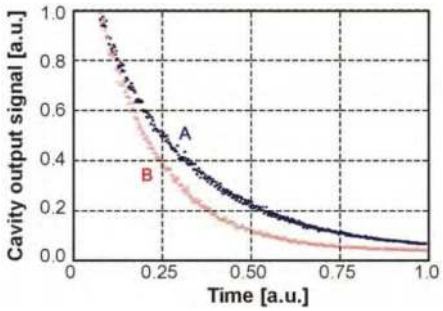

Fig. 8. Examples of signals at the output of the optical cavity without absorber (A) and at the output of the cavity filled with absorber (B)

Based on equation (4) and (5), the lowest concentration (concentration limit) of analyzed gas molecules (C_{lmt}), which causes a measurable change of the output signal, can be determined from the formula

$$C_{lmt} = \frac{1}{c\sigma\tau_0}\delta_\tau = \frac{(1-R)}{\sigma \cdot L}\delta_\tau \,, \tag{7}$$

where δ_τ is the relative precision of the decay time measurement (uncertainty). The relationship between uncertainty δ_τ and τ_0 can be described as

$$\delta_\tau = \frac{\tau_0 - \tau_{lmt}}{\tau_0} \cdot 100\% \,, \tag{8}$$

where τ_{lmt} denotes a decay time for minimal absorber concentration.
In the other hand, C_{lmt} can be treated as the detection limit of the sensor. It is a function of two variables: the decay time for the empty cavity (τ_0) and uncertainty (δ_τ). Furthermore, the decay time τ_0, according to the formula (6), depends on the length of the resonator and the reflectivity mirrors. The longer this time, the longer effective path of absorption, the greater the sensitivity of the sensor and the lower concentrations of the absorber can be measured.
Another way of gas concentration determination is measurements of the phase shift between the respective harmonics of the signal (e.g. the first) at the input and output optical cavity [Herbelin et al. 1980, Engeln et al. 1996]. In these measurements, lock-in amplifiers are frequently used. The phase shift occurs due to cavity ability to the energy (radiation) storage, as in the case of the charging process of the capacitor. The value of $tan(\varphi)$ is associated with the decay of radiation in the cavity dependence

$$tan(\varphi) = 4\pi f \tau \,, \tag{9}$$

where f denotes the modulation frequency. The gas concentration can be calculated by comparing the phase (φ) when the resonator is filled with test gas and the phase shift (φ_0) for the resonator without gas

$$C = \frac{4\pi f}{c\sigma}\left(\frac{1}{tg(\varphi)} - \frac{1}{tg(\varphi_0)}\right). \tag{10}$$

In techniques with an off-axis arrangement light source and optical cavity, the gas concentration is often determined by measuring the amplitude of the signal from the photodetector. Application of the system synchronization of laser and cavity modes is not required. It simplifies the experimental system. Thanks to this, the intensity from individual reflections of radiation from the output mirror can be summed [O'Keefe et al., 1999, O'Keefe, 1998]

$$I_{os} = -I_{in}\frac{(1-R)^2 e^{-\alpha L}}{2\ln(R\cdot e^{-\alpha L})}. \tag{11}$$

In the case of a single pass, the transmitted light pulse is described by

$$I_{op} = I_{in}(1-R)^2 e^{-\alpha L}. \tag{12}$$

Comparing expressions (11) and (12) it can be shown that for small absorption coefficients a and high reflectivity mirrors ($R \to 1$) ratio of the I_{OS}/I_{OP} can be expressed with the formula

$$\frac{I_{os}}{I_{op}} = -\frac{1}{2\left[\ln(R)-\alpha L\right]} \to \frac{1}{2(1-R+\alpha L)}, \tag{13}$$

thus

$$C = \frac{\ln(R)}{\sigma\cdot L}\frac{I_{os}-I_{op}}{I_{os}}. \tag{14}$$

An important drawback of this method is the necessity of knowledge of the mirrors reflectivity to determining the gas concentration. In practical realisations it is difficult to ensure.

4. NO_x sensors project

Basic experimental setups of the cavity enhanced methods were described in the third section. All of them consist of pulse laser (or cw laser with modulator), beam directing and shaping system (mirrors, diaphragms, diffraction grating), optical cavity and photoreceiver with signal processing system (e.g. digital oscilloscope in the simplest case). First of all, the sensor project should take into account the appropriate matching cavity parameters and the laser emission wavelength to the test gas absorption spectrum (Fig. 9).

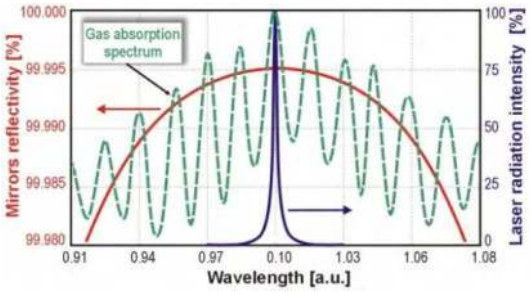

Fig. 9. Illustration of matching the laser emission wavelength and cavity mirrors transmission.

Moreover, it is necessary to apply adequate optical cavity, which provides repeatedly reflection of the laser radiation. To ensure multiple reflections, the cavity must be stable, i.e. the light after reflection from the mirrors must be re-focused (Fig. 10.a). In the case of an unstable cavity, the laser beam after a few reflections leaves the cavity, and thus there are large losses (Fig. 10.b).

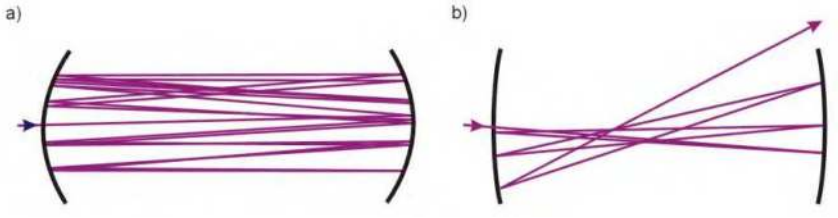

Fig. 10. Schematic illustration of the reflections in stable cavity (a) and in unstable one (b).

For the cavity to be stable, the selected curvature rays of the mirrors (r_1, r_2) and the distance between them (L) should be appropriate. The relation between these parameters describes the so-called stability criterion [Busch & Bush, 1999]

$$0 \le g_1 \cdot g_2 \le 1 , \tag{15}$$

where the parameters g_1 and g_2 are respectively

$$g_1 = \left(1 - \frac{L}{r_1}\right), \tag{16}$$

$$g_2 = \left(1 - \frac{L}{r_2}\right). \tag{17}$$

The optical signal from the cavity is registered with a photoreceiver, the operating spectrum of which should be matched to the selected absorption line of the gas. It usually is characterized by high gain, high speed and low dark current. In addition to the photodetector, the photoreceiver frequently includes different type of preamplifier which is used to amplify the signal from the photodetector. The preamplifier should have a wide dynamic range, low noises, high gain and an appropriately selected frequency band [Rogalski & Bielecki, 2006]. Next, the signal from the preamplifier is digitized with a high sampling rate (e.g. 100 MS/s). Data from the analogue-to-digital converter (ADC) are transmitted to a computer, for example through a USB interface. Special computer software provides processing of the measuring data and gas concentration determination. A scheme of a signal processing in the cavity enhanced sensor is presented in Fig. 11.

Observation of NO_x molecules can be done at electronic transitions which are characterized by a broad absorption spectra providing a relatively large mean absorption cross section within the range of several nanometres. Therefore the use of broadband multimode lasers is possible. In the case of nitrogen dioxide, the absorption spectrum has a band in the 395 - 430 nm range with a mean cross section of about $6 \cdot 10^{-19}$ cm^2 (Fig. 12a). There are various light sources applied, e.g. blue – violet LED's or diode lasers or even broadband supercontinuum sources [Wojtas et al., 2009, Holc et al., 2010, Stelmaszczyk et al., 2009].

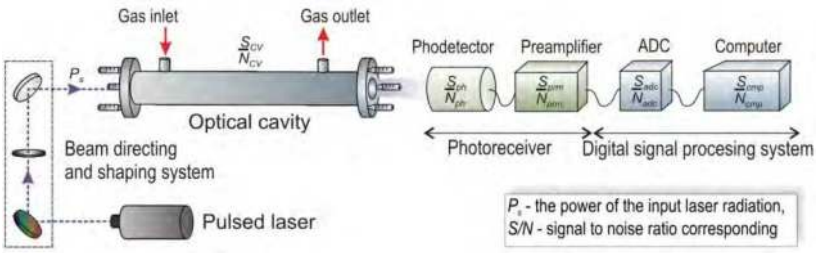

Fig. 11. Block diagram of NO_x sensor.

Assuming that determination of the gas concentration basis on the temporal analysis, the sensor sensitivity (in generally) depends on the mirrors reflectivity, cavity length and uncertainty of decay time measurements (Fig. 12b). The sensitivities of the laboratory NO_2 sensors reach 0.1 ppb. Our approaches to the nitrogen dioxide sensor were already described in several papers [Wojtas et al., 2006, Nowakowski et al., 2009].

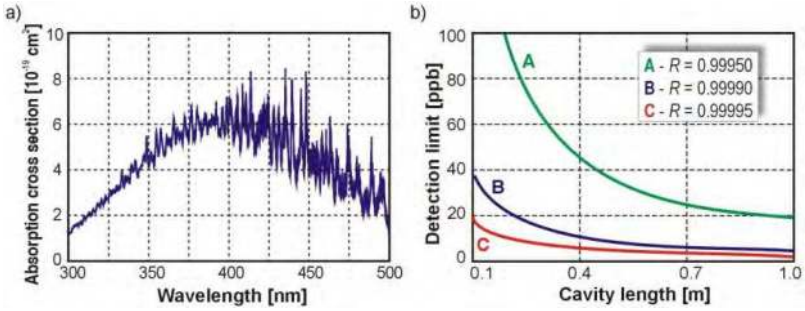

Fig. 12. NO_2 absorption spectrum (a) and dependence of the concentration limit on the cavity length and the reflectivity of mirrors *R* (b).

However, for many other compounds (like N_2O and NO) the electronic transitions correspond to the ultraviolet spectral range [HITRAN, 2008], where neither suitable laser sources nor high reflectivity mirrors are available. For example, reflectivities of available UV mirrors do not exceed the value of 90%. Therefore, a higher sensitivity of the NO and N_2O sensor can be obtained using IR absorption lines (Fig. 13).

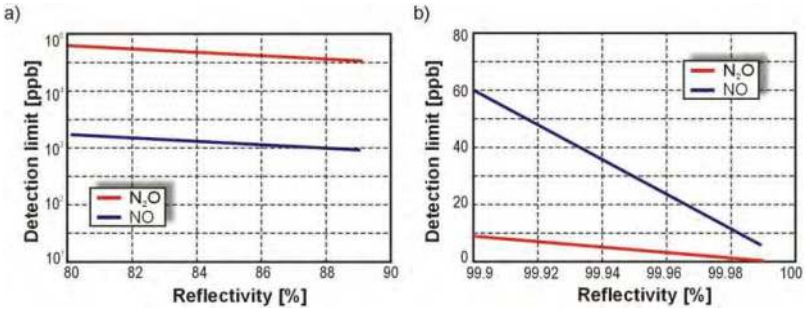

Fig. 13. Detectable concentration limit versus cavity mirrors reflectivity in UV (a) and in IR wavelength ranges (b).

The analyses show that the IR wavelength range provides the possibility to develop NO and N_2O sensor, the sensitivity of which could reach the ppb level (Rutecka, 2010). For instance, at the wavelength ranges of 5.24 μm – 5.28 μm and 4.51 μm – 4.56 μm the absorption cross section reaches the value $3.9x10^{-18}$ cm² for N_2O and $0.7\ x10^{-18}$ cm² for NO. Additionally, there is no significant interference of absorption lines of other atmosphere gases (e.g. CO, H_2O). There could only be observed a low interference of H_2O, which can be minimized with the use of special particles of a filter or dryer. Both NO and N_2O absorption spectrum are presented in Fig. 14 and in Fig. 15 respectively.
In this spectral range, quantum cascade lasers (QCL) are the most suitable radiation sources for experiments with cavity enhanced methods. Available QCL's provide high power and narrowband pulses of radiation [Namjou et al., 1998, Alpes Lasers SA]. The *FWHM* duration time of their pulses reaches hundreds of microseconds pulses while the repetition rate might be of some kHz. Moreover, their emission wavelength can be easy tuned to the maxima of N_2O and NO absorption cross section.

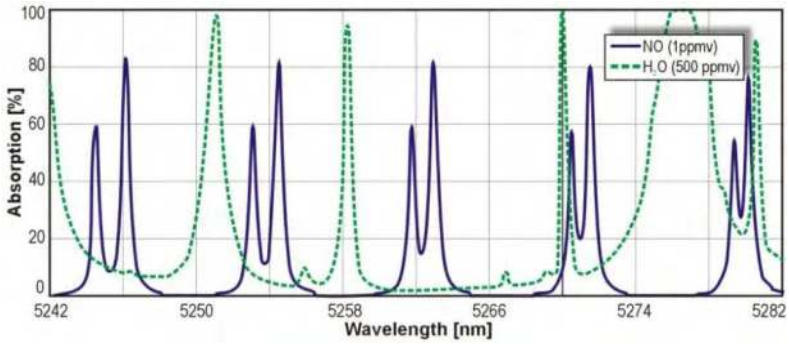

Fig. 14. NO absorption spectrum [Hitran, 2008].

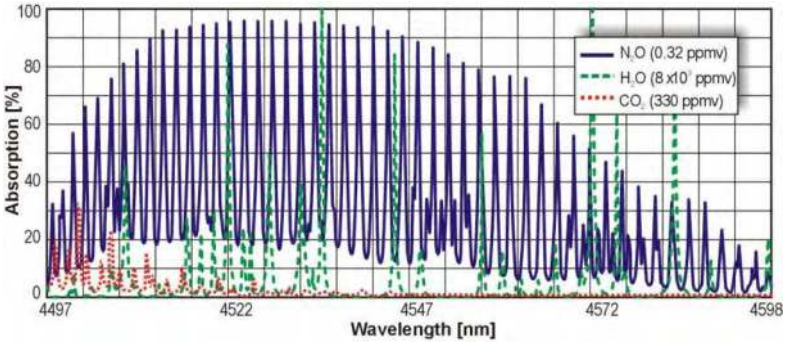

Fig. 15. N_2O absorption spectrum [Hitran, 2008].

5. Signal to noise ratio of the sensor

As we have seen, the reflectivity of the mirrors has a significant impact on the theoretical sensitivity of the sensor. According to the equation (7), the sensor sensitivity is higher when

the mirror reflectivity and cavity length are increased (Fig. 12 and Fig. 13). However, then a lower level of optical signal reaches the photodetector. Therefore, the signal-to-noise ratio (*SNR*) of the system is very important.

5.1 Optical cavity parameters

Usually, for the cavities, such parameters like, e.g., the finesse F, the time of a photon life τ_p, the transmission function $T(R,\lambda)$ and signal-to-noise ratio S_{cv}/N_{cv} are determined [Wojtas & Bielecki, 2008].

The finesse F characterizes the quality of the cavity and determines an effective number of a roundtrip of optical radiation in the cavity up to its energy reaching the level of $1/e$. The finesse F can be found from the formula

$$F = \pi \frac{\sqrt{R}}{1-R}. \tag{18}$$

The time of a photon life is described by the equation

$$t_p = \frac{2nLF}{c}, \tag{19}$$

where n is the refractive index. The transmission function of the optical cavity is known as the Airy formula. It has the following form

$$T(R,\phi) = \frac{(1-R)^2}{(1-R)^2 + 4R\sin^2(\frac{\phi}{2})}, \tag{20}$$

where ϕ is the radiation phase shift during one roundtrip inside the cavity

$$\phi = \frac{4\pi nL}{\lambda}, \tag{21}$$

and λ is the optical radiation wavelength. The graphical representation of Eq. (20) is presented in Fig. 16.

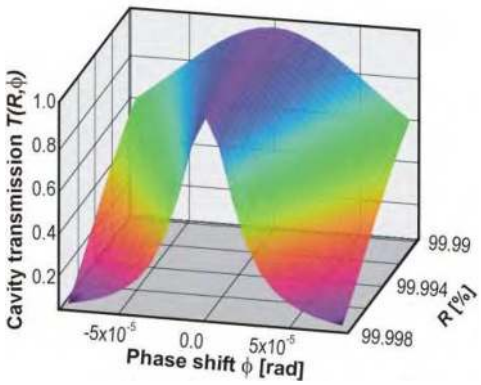

Fig. 16. Graphical representation of the transmission function of an optical cavity.

It shows a strong influence of the mirrors reflectivity on the selectivity of an optical cavity. The transmission of the cavity is maximum wherever ϕ is the integral multiple of 2π.
The optical cavity signal-to-noise ratio (S_{cv}/N_{cv}) is connected with its transmission function. S_{cv}/N_{cv} is directly proportional to the power of radiation matched to the transmission function of a cavity and to an absorption band of the examined gas. However, S_{cv}/N_{cv} is inversely proportional to the power of undesirable radiation transmitted through a cavity because of non-zero values of the mirrors' transmissions. The formula describing a signal-to-noise ratio of the cavity is

$$\frac{S_{cv}(\lambda)}{N_{cv}(\lambda)} = \frac{\left[T(R(\lambda),\phi)\right]^2}{\left[1-R(\lambda)\right]^2}. \tag{22}$$

Assuming that a length of optical cavity is 0.5 m and it is consists of two concave mirrors with the reflectivity of 0.999976, then $S_{cv}/N_{cv}=1.7\times10^9$ ($F = 1.3\times10^5$, $\tau_f=5.2\times10^{-4}$s).

5.2 Analysis of detection system parameters

Due to the high value of *SNR* of the optical cavity, the signal-to-noise ratio of an electronic circuit is the crucial parameter of the cavity enhanced sensor. The signal from the cavities is registered with different types of photodetectors; depending on the spectral range. In the case of ultraviolet (UV), visible (VIS) and near infrared (NIR) region (approximately from form 100 nm up to 1.5 μm) the most popular are photomultiplier tubes (PMT's). They are characterized by high gain, high speed and low dark current. Because of PMT high resistance, transimpedance preamplifiers are usually used to amplify signal from PMT. They are characterized by a wide dynamic range [Rogalski & Bielecki, 2006].
In the medium infrared (MIR) part of the spectrum there are two types of photodetectors: thermal and quantum. Thermal photodetectors use infrared energy as heat, and their responsitivity is independent of the wavelength. But they have disadvantages because their response time is slow and detectivity is low. Therefore, quantum photodetectors are used in the practical implementations of cavity enhanced methods. They offer higher responsitivity and faster response speed. To achieve higher performance, i.e. a wider frequency band and higher detectivity (D^*), they are cooled. There are several cooling methods: thermoelectric cooling (TEC), cryogenic cooling (e.g. dry ice or liquid nitrogen) and mechanical cooling (e.g. Stirling coolers). The most popular are HgCdTe (mercury-cadmium-telluride, MCT) photoconductive and photovoltaic detectors. There are available MCT photodetectors that use monolithic optical immersion technology and TEC cooling. They offer high detectivity (about 10^{12} cm·√Hz/W) and high speed (up to 1GHz). To amplify the signal from the MCT photodetector, transimpedance preamplifiers are applied as well [Hamamatsu, 2011, Piotrowski et al., 2004, VIGO System S.A.].

5.2.1 Photoreceiver with photomultiplier tube

To determine the signal-to-noise ratio of the photoreceiver, the PMT equivalent scheme is necessary. The scheme is presented in Fig. 17. The current source I_s represents the current of useful signal, R_p and C_p are the resistance and capacitance of the photomultiplier respectively [Wojtas et al., 2008].
PMT noise sources are as follows: the current source I_{ns} represents the shot noise from useful signal, the current source I_{nd} represents shot noise of anode dark current, I_{nb} is the current sources of noise from background radiation and I_{nRL} is the thermal noise of load resistance.

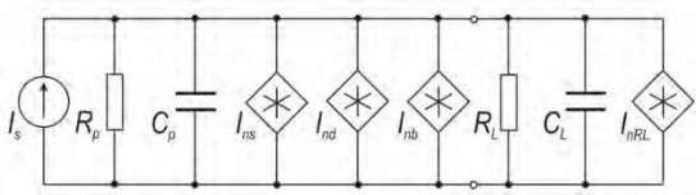

Fig. 17. PMT equivalent scheme.

In the case when all the described noise sources will be taken into consideration, PMT signal-to-noise ratio can be determined by the formula [Wojtas & Bielecki, 2008]

$$\frac{S_{ph}}{N_{ph}} = \frac{I_s^2}{I_{ns}^2 + I_{nd}^2 + I_{nb}^2 + I_{nRL}^2}. \tag{23}$$

Assuming that during cavity enhanced experiments background noise can be eliminated, and a photoemission process is described by the Poisson model, and all stages of PMT will have the same gain, then

$$\frac{S_{ph}}{N_{ph}} = \frac{(P_s \cdot S_p \cdot G_p)^2}{2\,q\,\Delta\,f_n\,(G_p\,S_p\,P_s + I_{da})\frac{\delta}{\delta - 1} + \frac{4\,k\,T_o\,\Delta\,f_n}{R_L}}, \tag{24}$$

where P_s is the power of optical radiation, G_p is the PMT gain, S_p is the photocathode sensitivity, q is the electron charge, Δf_n is the noise bandwidth, I_{da} is the anode dark current, δ is one stage of the PMT gain, k is the Boltzmann constant, and T_0 is the temperature [Flyckt & Marmonier, 2002].
The noise bandwidth can be determined from the formula

$$\Delta f_n = \frac{\pi}{2}\Delta f_{3dB} \approx \frac{1}{4R_L(C_L + C_p)}, \tag{25}$$

where Δf_{3dB} represents 3dB frequency bandwidth.
Because PMT can be treated as a current source the best preamplifier configuration is a transimpedance preamplifier. Moreover, its input circuit does not affect photodetector polarization. The scheme of a transimpedance preamplifier is presented in Fig. 18.
In the case when one photoelectron is emitted by the PMT photocathode, the output voltage signal of the transimpedance preamplifier can be described by the formula

$$V_{prm} = \frac{q \cdot G_p \cdot R_f}{R_f \cdot C_{eq}' - t_i} \cdot \left[\exp\left(\frac{-t}{R_f \cdot C_{eq}'} \right) - \exp\left(\frac{-t}{t_i} \right) \right], \tag{26}$$

where C_{eq}' is PMT and a load circuit equivalent capacitance located in the feedback circuit, and t_i is PMT pulse duration. The Miller theorem states that C_{eq}' is (G_{OL} + 1) times lower then C_{eq} (G_{OL} is the amplifier open-loop gain). In the appropriate developed circuit, the value of C_{eq}' is lower than 0.1 pF.

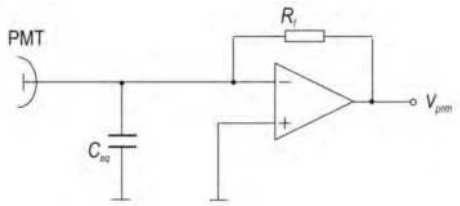

Fig. 18. Scheme of the transimpedance preamplifier.

Analysis showed that an increase in R_f caused that the output pulse duration is longer and longer (Fig. 19). Because of this, to reach a high value of gain and to avoid signal distortion, the next stage of amplifier should be used. Because of the low output resistance of the transimpedance preamplifier (< 50 Ω), a voltage amplifier can be used.

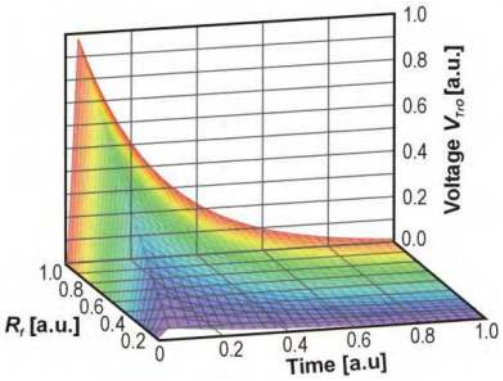

Fig. 19. Example of transimpedance preamplifier output signal.

To determine the *SNR* of the photoreceiver, an equivalent scheme is necessary (Fig. 20).

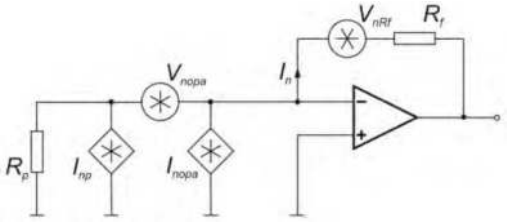

Fig. 20. Equivalent scheme of the first stage of the photoreceiver.

The noise of the operational amplifier is represented by the voltage source V_{nopa} and the current source I_{nopa}. The noise source I_{nph} is equivalent to the PMT noise. In this case, the total current noise I_{nt} is described by the formula

$$I_{nt}^2 = I_{np}^2 + \left(V_{nopa} \frac{R_p + R_f}{R_p R_f} \right)^2 + I_{nopa}^2 + \left(\frac{V_{nRf}}{R_f} \right)^2, \tag{27}$$

where V_{nRf} is the thermal noise determined by the equation

$$V_{nRf}^2 = 4kT_o R_f \Delta f_n . \tag{28}$$

The output voltage noise of the transimpedance preamplifier can be defined as

$$V_{nprm} = I_{nt} R_f , \tag{29}$$

and of the *SNR* of the photoreceiver can be described with the formula

$$\left(\frac{S_{prm}}{N_{prm}} \right)_{pmt} = \frac{I_s^2}{I_{nt}^2}. \tag{30}$$

Usually, the amplified signal from the preamplifier is fed to an analogue digital converter (ADC). This circuit also adds its noise. Assuming a 12-bit ADC and the same quantization steps δ_{adc}, its noise can be determined by the formula

$$V_{nadc}^2 = \frac{{\delta_{adc}}^2}{12}. \tag{31}$$

The analysis showed that the *SNR* of the detection system consists of PMT, preamplifier and ADC, and can be described by the formula

$$\left(\frac{S_{adc}}{N_{adc}} \right)_{pmt} = \frac{\left(P_s S_p G_p \right)^2 \cdot R_f^2}{\gamma R_f^2 \Delta f_n + V_{nadc}^2}, \tag{32}$$

where

$$\gamma = 2q(G_p S_p P_s + I_{da}) \frac{\delta}{\delta - 1} + \left(V_{nopa} \frac{R_p + R_f}{R_p \cdot R_f} \right)^2 + I_{nopa}^2 + \frac{4kT_o}{R_f} . \tag{33}$$

5.2.2 Photoreceiver with a MCT photodiode

The noise equivalent scheme of the photoreceiver using a MCT photodiode and a transimpedance preamplifier is presented in Fig. 21. The signal current generator I_{ph} represents the detected signal. Noises in a photodiode are represented by three noise generators: I_{nph} - the shot noise associated with photocurrent, I_{nd} - the shot noise of a dark current, while I_{nb} - the shot noise from a background current [Bielecki 2002].
In the scheme, the value of the load resistance of the photodetector depends on the feedback resistance R_f and the preamplifier gain *G*. The resistor R_f affects both the level of the preamplifier output signal and its noise. The noise current generator I_{nf} is the thermal noise current and excess noise of the feedback resistance. Since the thermal noise of I_{nf} is inversely related to the square root of the resistance, R_f should be of great value. The R_{sh} is the shunt

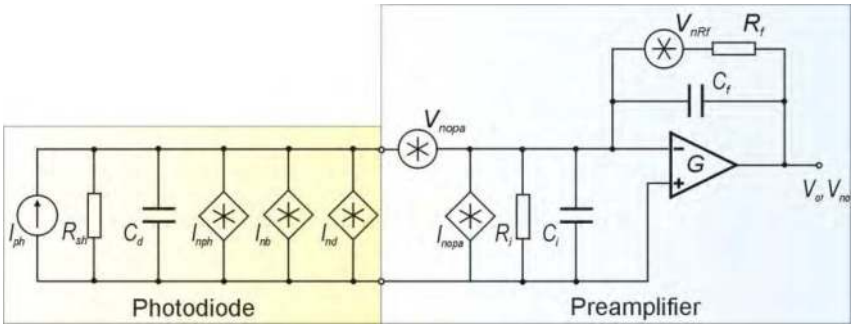

Fig. 21. Scheme of the photoreceiver with a photodiode.

resistance of a photodiode. The equivalent photoreceiver noise is the square root of each component noise squares sum [Bielecki et al., 2009]. Thus, the signal-to-noise ratio can be described with the simplified expression

$$\left(\frac{S_{prm}}{N_{prm}}\right)_{pht} = \frac{I_{ph}^2}{\left(I_{nph}^2 + I_{nd}^2 + I_{nb}^2 + I_{nopa}^2 + \frac{4kT\Delta f}{R_f}\right) + \left(V_{nopa}\frac{R_{eq}^2}{1+\omega^2\tau_{eq}^2}\right)^2}, \tag{34}$$

where

$$R_{eq} = \frac{R_f R_{sh}}{R_f + R_{sh}} \quad \text{and} \quad \tau_{eq} = R_{eq}\left(C_f + C_d\right). \tag{35}$$

Only the modulus of feedback loop impedance and photodetector impedance is included. Furthermore, it could be assumed that in experiments applying cavity enhanced methods, current I_{nb} can be ignored. Moreover, intensity of the radiation reaching the photodiode is rather low, thus shot noise associated with the photocurrent is negligibly. In practical realisations (low frequency and R_{sh}>>R_f), the *SNR* of the system consisting in a photodiode, preamplifier and ADC can be determined from equation

$$\left(\frac{S_{adc}}{N_{adc}}\right)_{pht} = \frac{\left(R_i P_s\right)^2}{\left(\frac{R_i (A\Delta f)^{1/2}}{D^*}\right)^2 + I_{nopa}{}^2 + \frac{4kT\Delta f}{R_f} + \left(\frac{V_{nopa}}{R_f}\right)^2 + V_{nadc}^2}, \tag{36}$$

where R_i - photodiode current responsitivity, A – detector active area.

5.3 Methods of SNR improving

Analyses in the previous section showed a significant influence of preamplifier feedback resistance (R_f) on the output photoreceiver signal. In an appropriately developed photoreceiver, the preamplifier shouldn't degrade photoreceiver performance. In Fig. 22 ADC noise, preamplifier noise and photodetector noise for different values of R_f were presented.

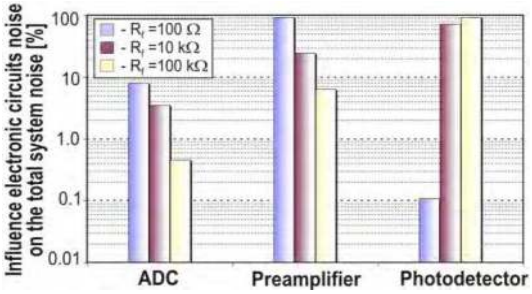

Fig. 22. Comparison noise sources of electronic circuit for different values of R_f.

In the case of R_f = 100 Ω, the highest influence on the total electronic system noise was preamplifier noise at ~92%. However, an increase in R_f caused a decrease in influence preamplifier noise on the total signal processing system noise. For R_f = 100 kΩ, the noise of photodetector is equal to ~93% of the total signal processing system noise and preamplifier is only ~6%. ADC noise is below 8%. Furthermore, the value of R_f also has a strong influence on the bandwidth of the system. In Fig. 23, the dependence *SNR* of the signal processing system and a preamplifier output pulse fall time on the R_f is presented.

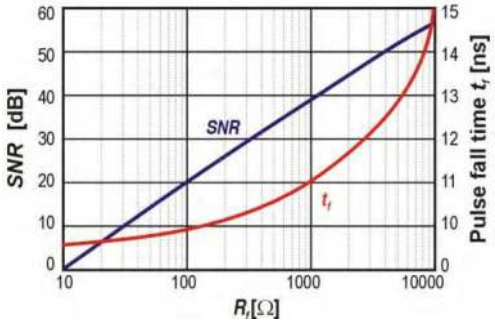

Fig. 23. Dependence of electronic circuit *SNR* and fall time of output pulse on resistance R_f.

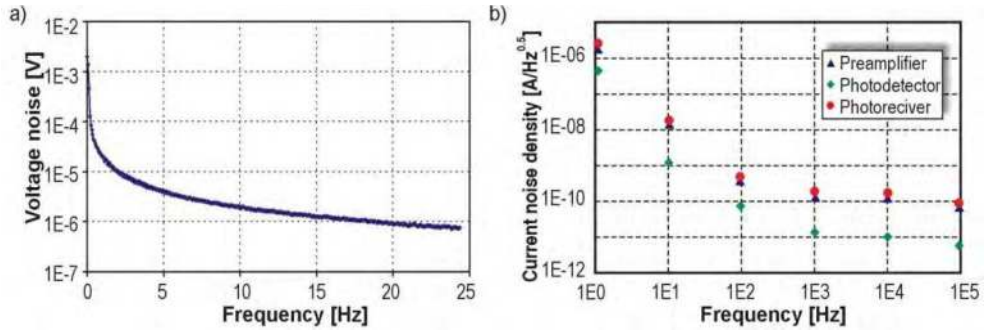

Fig. 24. Voltage noise (a) and current noise density (b) of the photoreceiver.

Experiments have shown that in the low frequency region the *1/f* noise is dominant (Fig. 24a). Therefore, in order to minimize the adverse impact of such noise on the detectivity of the receiver (and *SNR* as well), a high pass filter is frequently used which limits the frequency bandwidth by several kilohertz. In the higher frequency region, there is dominant *g-r* noise by recombination of electrons and holes. Although the density of this noise is less than *1/f* (Fig. 24b), the upper limit frequency should be suitably matched to the recorded signal bandwidth to avoid *SNR* degradation.
SNR of the cavity enhanced system can be additionally improved by the use of one of the advanced methods of signal detection, i.e. coherent averaging [Lyons, 2010]. This technique can be implemented in the software of the digital signal processing system. The software is usually installed in a personal computer. Thanks to this, increase in the *SNR* is directly proportional to the root of a number of the averaging samples n_{smpl},

$$\frac{S_{cmp}}{N_{cmp}} = S_{adc}\left(\frac{N_{adc}}{\sqrt{n_{smpl}}}\right)^{-1}. \tag{37}$$

Thanks to improving *SNR*, uncertainty of decay time determination is likely to reach values below 0.5% (e.g. in the case of 10 000 averaging samples). Hence, the detection limit can achieve the value of about 2×10^{-9} cm^{-1} (Fig. 25).

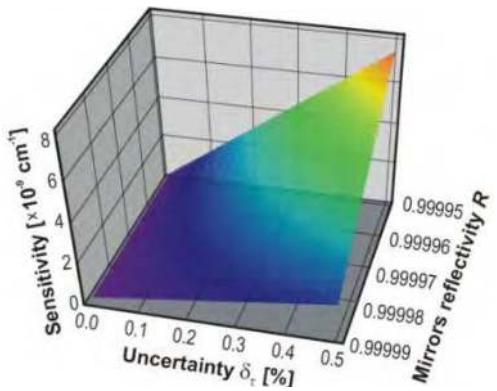

Fig. 25. Dependence cavity enhanced sensor sensitivity on decay time precision determination and cavity mirrors reflectivity.

6. Conclusion

In this chapter, characterisations of absorption spectroscopy methods were shown. The methods provide the possibility of absorption spectra investigations. This kind of spectra can be defined as the set of all electron crossings from lower energy levels to higher ones. They caused an increase in molecules energy. In practical implementations, a source of radiation and very sensitive photoreceiver is used which records radiation passing through the absorber sample. One of the most common gas detection systems is differential optical absorption spectroscopy. Such arrangements are applied to the monitoring of atmospheric pollutants, including the detection of NO_x, in terrestrial applications, in air and in space, e.g. GOME and SCIAMACHY satellite.

Cavity enhanced spectroscopy is the one of the most sensitive absorption methods. The greatest sensitivity is provided by P-CRDS, CW-CRDS and CEAS methods. CRDS was applied to determine the mirrors reflectivity for the first time in the early 1980's. This method provides a much higher sensitivity than conventional absorption spectroscopy. An optical cavity with a high quality is applied that is made up of two concave mirrors with very high reflectance R. This results in a long optical path, even up to several kilometres. To determine the gas concentration several different methods are used: by measuring the decay time of the signal, by measuring the phase shift, and by measuring the signal amplitude. All of them were described in detail.

Furthermore, the basic experimental setups of cavity enhanced methods were described. Generally, they consist of pulse laser (or cw laser with modulator), beam directing and shaping system (mirrors, diaphragms, diffraction grating), optical cavity and photoreceiver with signal processing system (e.g. digital oscilloscope in the simplest case). First of all, the sensor project should take into account the appropriate matching cavity parameters and the laser emission wavelength to the test gas absorption spectrum.

Observation of NO_x molecules can be done at electronic transitions which are characterized by a broad absorption spectra providing a relatively large mean absorption cross section within the range of several nanometres. Therefore, using broadband multimode lasers is possible. However, for many other compounds (like N_2O and NO), the electronic transitions correspond to an ultraviolet spectral range, where neither suitable laser sources nor high reflectivity mirrors are available. Therefore, a higher sensitivity of the NO and N_2O sensor can be obtained using an IR absorption line.

It was shown that reflectivity of the mirrors has a significant impact on the theoretical sensitivity of the sensor. The sensor sensitivity is higher when the mirror reflectivity and cavity length are increased. However, then a lower level of optical signal reaches the photodetector. Therefore, the signal-to-noise ratio of the system is very important. Thus analyses of the main parameters of the optical cavity, photoreceiver and the signal processing system were performed. In the analyses the most popular photodetectors were taken into consideration. In the UV, VIS and NIR spectral regions, the photomultiplier is characterized with high performance. Photodetectors designed for MIR operation require an additional cooling system. Thanks to this they can achieve a higher performance, i.e. a wider frequency band and higher detectivity (D^*). Because of the many advantages, MCT photodetectors are frequently used in cavity enhanced applications.

Analyses showed a significant influence of preamplifier feedback resistance (R_f) on the output photoreceiver signal. In appropriately developed photoreceiver, the preamplifier shouldn't degrade photoreceiver performance. The *SNR* of the cavity enhanced system can be additionally improved by the use of one of the advanced methods of signal detection, i.e. coherent averaging.

Cavity enhanced sensors are able to measure NO_x concentration at ppb level. Their sensitivity is comparable with the sensitivities of instruments based on other methods, e.g. gas chromatography or mass spectrometry. The developed sensor can be applied for monitoring atmosphere quality. Using the sensor, the detection of vapours from some explosive materials is also possible.

7. Acknowledgment

The researchers are supported by the Ministry of Science and High Education of Poland in 2009-2011.

8. References

Alpes Lasers SA, 1-3 Max.-de-Meuron, C.P. 1766, CH-2001 Neuchâtel, http://www.alpeslasers.ch/products.html#products_top

Atherton, K.J., Yu, H., Stewart, G. & Culshaw, B. (2004). Gas detection with fibre amplifiers by intra-cavity and cavity ring-down absorption, *Measurement Science and Technology* Vol. 15, pp. 1621–1628

Berden, G., Peeters, R. & Meijer, G. (2000). Cavity ring-down spectroscopy: Experimental schemes and applications, International Reviews In Physical Chemistry, Vol. 19, No. 4. pp. 565-607

Bielecki, Z. (2002). Maximization of signal to noise ratio in infrared radiation receivers, *Opto-Electron. Rev.*, 10, pp. 209-216

Bielecki, Z., Kolosowski, W., Sedek, E., Wnuk, M. & Wojtas, J. (2009). Multispectral detection circuits in special application, *Transactions on Modelling and Simulations*, WIT Press – WIT, Vol 48, Print ISBN: 1-84564-187-0; On-line ISBN: 1-84564-364-5; Print ISSN: 1746-4064, pp. 217-228

Busch, K.W., Busch, M.A. (1999). *Cavity-Ringdown Spectroscopy*, ACS Symposium series, American Chemical Society, Washington DC

Chudzynski, S., Czyzewski, A., Skubiszak, W., Stacewicz, T., Stelmaszczyk, K., Szymanski, A. & Ernst, K. (1999). Practical solutions for calibration of DIAL system, Optica Applicata 29, pp. 477 – 485

Courtillot I., Morville J., Motto-Ros & Romanini D. (2006). Sub-ppb NO2 detection by optical feedback cavity-enhanced absorption spectroscopy with a blue diode laser. *Appl. Phys. B*, 85, pp. 407–412

Czyzewski, A., Chudzynski, S., Ernst, K., Karasinski, G., Kilianek, L., Pietruczuk, A., Skubiszak, W., Stacewicz, T., Stelmaszczyk, K., Koch, B. & Rairoux, P. (2001). Cavity Ring-Down Spectrography, *Optics Commun*, 191, 271 – 275

Drescher, S.R., Brown, S.D. (2006). Solid phase microextraction-gas chromatographic-mass spectrometric determination of nitrous oxide evolution to measure denitrification

in estuarine soils and sediments, *Journal of Chromatography A*, 1133(1–2), pp. 300–304

Engeln, R., Berden, G. & Meijer, G. (1996). Phase shift cavity ring down absorption spectroscopy, *Chemical Physic Letters*, 262, pp. 105 – 109

Engeln, R., Berden, G., Peeters, R. & Meijer, G. (1998). Cavity enhanced absorption and cavity enhanced magnetic rotation spectroscopy, *Review Of Scientific Instruments*, Vol. 69, No. 11, pp. 3763 – 3769

Flyckt, S.O., Marmonier, C. (2002). *Photomultiplier tubes, principles, and applications*, Photonics, Brive, France

Godish, T. (2004). *Air Quality*, Lewis Publishers, ISBN 156670586X, 9781566705868

Grossel, A., Ze´ninari, V., Joly, L., Parvitte, B., Durry, G. & Courtois, D. (2007). Photoacoustic detection of nitric oxide with a Helmholtz resonant quantum cascade laser sensor, *Infrared Physics & Technology*, 51, pp. 95–101

Hamamatsu, Solid State Division (2011). *Technical information SD-12, Characteristics and use of infrared detectors*, Cat. No. KIRD9001E04, Mar. 2011 DN

He, Y., Orr, B.J. (2000). Ringdown and cavity-enhanced absorption spectroscopy using a continuous-wave tunable diode laser and a rapidly swept optical cavity, *Chemical Physics Letters*, 319, pp. 131–137

Herbelin, J.M., McKay, J.A.., Kwok, M.A., Ueunten, R.H., Urevig, D.S., Spencer, D.J. & Benard, D.J. (1980). Sensitive measurement of photon lifetime and true reflectances in optical cavity by a phase-shift method, *Applied Optics*, Vol. 19, Issue 1, pp. 144-147

HITRAN (2008). High-resolution transmission molecular absorption database, http://www.hitran.com

Holc, K., Bielecki, Z., Wojtas, J., Perlin, P., Goss, J., Czyzewski, A., Magryta, P. & Stacewicz, T. (2010). Blue laser diodes for trace matter detection, *Optica Applicata*, Vol. XL, No. 3, 2010, pp. 641-651

Horii, C.V., Zahniser, M.S., Nelson, D.D., McManus, J.B. & Wofsy, S.C. (1999). Nitric Acid and Nitrogen Dioxide Flux Measurements: a New Application of Tunable Diode Laser Absorption Spectroscopy, *Proc.SPIE*, v. 3758, pp. 152-161

Jean-Franqois, D., Ritz, D. & Carlier, P. (1999). Multiple-pass cell for very-long-path infrared spectrometry, Applied Optics, Vol. 38, No. 19, pp. 4145-4151

Kasyutich, V.L., Bale, C.S.E., Canosa-Mas, C.E., Pfrang, C., Vaughan , S. & Wayne, R.P. (2003a). Off-axis continuous-wave cavity-enhanced absorption spectroscopy of narrow-band and broadband absorbers using red diode lasers, *Applied Physics B*, Vol. 75, pp. 755-761

Kasyutich, V.L., Bale, C.S.E., Canosa-Mas, C.E., Pfrang, C., Vaughan, S. & Wayne, R.P. (2003b). Cavity-enhanced absorption: detection of nitrogen dioxide and iodine monoxide using a violet laser diode, *Applied Physics B*, Vol. 76, No. 6, pp. 691-698

Karasinski, G., Kardas, A.E., Markowicz, K., Malinowski, S.P., Stacewicz, T., Stelmaszczyk, K., Chudzynski, S., Skubiszak, W., Posyniak, M., Jagodnicka, A.K., Hochhertz, C. & L. Woeste (2007). LIDAR investigation of properties of atmospheric aerosol, *The European Physical Journal Special Topics*, 144, pp. 129−138

Lagalante, A.F. (1999). Atomic Absorption Spectroscopy: A Tutorial Review, *Applied Spectroscopy Reviews*, Vol. 34(3), pp.173–189

Li, P., Shi, K. & Liu, Z. (2005). Optical scattering spectroscopy by using tightly focused supercontinuum, *Optics Express*, Vol. 13, No. 22, pp. 9039-9044

Lyons, R.G. (2010). *Understanding Digital Signal Processing*, Addison Wesley Pub Co Inc., 3rd Edition, ISBN-13: 978-0-13-702741-5, ISBN-10: 0-13-702741-9

Martin, R.V., Parrish, D.D., Ryerson, T.B., Nicks Jr., D.K., Chance, K., Kurosu, T.P., Jacob, D.J., Sturges, E.D., Fried, A. & Wert, B.P. (2004). Evaluation of GOME satellite measurements of tropospheric NO_2 and HCHO using regional data from aircraft campaigns in the southeastern United States, *Journal of Gophysical Research*, Vol. 109, 11 pp.

Mierczyk, Z., Zygmunt, M., Gawlikowski, A., Gietka, A., Kaszczuk, M., Knysak, P., Mlodzianko, A., Muzal, M., Piotrowski, W. & Wojtanowski, J. (2008). Two-wavelength backscattering lidar for stand off detection of aerosols, Lidar Technologies, Techniques, and Measurements for Atmospheric Remote Sensing IV. Edited by Singh, Upendra N.; Pappalardo, Gelsomina. *Proceedings of the SPIE*, Volume 7111, pp. 71110R-71110R-9

Moore, D.S. (2007). Recent Advances in Trace Explosives Detection Instrumentation, *Sens Imaging*, 8, pp. 9–38

Namjou, K., Cai, S., Whittaker, E.A., Faist, J., Gmachl, C., Capasso, F., Sivco, D.L. & Cho, A.Y. (1998) .Sensitive absorption spectroscopy with a room-temperature distributed-feedback quantum-cascade laser, *Optics Letters*, V23, 3, pp. 219 – 221

Noel, S., Bovensmann, H., Burrows, J.P., Frerick, Chance', J., K.V. & Goede, A.H.P. (1999). Global Atmospheric Monitoring with SCIAMACHY, *Physal. Chemical. Earth*, Vol. 24, No. 5, pp. 427-434

Nowakowski M., Wojtas J., Bielecki Z., & Mikolajczyk J. (2009). Cavity enhanced absorption spectroscopy sensor, Acta Phys. Pol. A, 116, 363–367

O'Keefe, A. (1998). Integrated cavity output analysis of ultra-weak absorption, *Chemical Physics Letters*, 293 (5-6), pp. 331-336

O'Keefe, A., Deacon, D.A.G. (1988). Cavity ring-down optical spectrometer for absorption measurements using pulsed laser sources, *Review of Scientific Instruments*, No. 59, pp. 2544-2554

O'Keefe, A., Scherer, J.J. & Paul, J.B. (1999). CW integrated cavity output spectroscopy, *Chemical Physic Letters*, 307 (5-6), pp. 343-349

Owsik J., Janucki J. (2004). Laser-induced breakdown spectrometer for non-destructive diagnostics", *Proc. SPIE*, 4962, pp. 135–142

Paul, J.B., Lapson, L. & Anderson, J.G. (2001). Ultrasensitive absorption spectroscopy with a high-finesse optical cavity and off-axis alignment, Applied Optics, Vol. 40, No. 27, pp. 4904-4910

Piotrowski A., Madejczyk P., Gawron W., Klos K., Romanis M., Grudzien M., Rogalski A. & Piotrowski J. (2004). MOCVD growth of Hg1xCdxTe heterostructures for uncooled infrared photodetectors. Opto-Electron. Rev., 12, pp. 453–458

Pipino, A.C.R. (1999). Ultrasensitive surface spectroscopy with a miniature optical resonator, *Physical Rewiew Letters*, Vol. 83, No. 15, pp. 3093-3096.

Rogalski, A., Bielecki, Z. (2006). Detection of optical radiation (chapter A1.4), *Handbook of optoelectronics*, Taylor & Francis, New York, London pp. 73-117

Romanini, D., Kachanov, A. A., Sadeghi, N. & Stoeckel, F. (1997). Diode laser cavity ring down spectroscopy, Chemical Physics Letters, No 270, pp. 538-545

Rutecka, B., Wojtas, J., Bielecki, Z., Mikołajczyk, J. & M. Nowakowski. (2010). Application of an optical parametric generator to cavity enhanced experiment. *Proc. of SPIE*, vol. 7745, pp. 77450I-1- 77450I-8

Saleh B.E.A., Teich M.C. (2007). *Fundamentals of Photonics*, John Wiley & Sons, 2nd Edition ISBN: 978-0-471-35832-9

Scherer, J.J., Paul, J.B., Jiao, H. & O'Keefe, A. (2001). Broadband ringdown spectral photography, *Applied Optics*, Vol. 40, No. 36, pp. 6725-6732

Shimadzu Scientific Instruments, 7102 Riverwood Drive, Columbia, MD 21046, Available from: http://www.mandel.ca/application_notes/SSI_GC_Green_Gasses_Lo. pdf

Sigrist, M.W. (1994). *Air monitoring by spectroscopic techniques*, John Wiley & Sons, ISBN-10: 0-471-55875-3. ISBN-13: 978-0-471-55875-0

Stelmaszczyk, K., Fechner, M., Rohwetter, P., Queißer, M., Czyzewski, A., Stacewicz, T. & L. Wöste, (2009). Towards Supercontinuum Cavity Ringdown Spectroscopy, *Appl. Phys. B*, 94, pp. 396–373

Stelmaszczyk, K., Rohwetter, P., Fechner, M., Queißer, M., Czyzewski, A., Stacewicz, T. & Wöste, L. (2009). Cavity Ring-Down Absorption Spectrography Based on Filament-Generated Supercontinuum Light, *Optics Express*, 17(5), 3673 – 3678

VIGO System S.A., http://www.vigo.com.pl/index.php/en/main_menu/strona_ glowna

Wang, P., Richter, A., Bruns, M., Burrows, J.P., Junkermann, W., Heue, K.P., Wagner, T., Platt, U. & Pundt, I. (2005). Airborne multi-axis DOAS measurements of tropospheric SO2 plumes in the Po-valley, Italy, *Atmosphric. Chemical. Physics Discussion*, No 5, pp. 2017–2045

Wojtas, J., Bielecki, Z. (2008). Signal processing system in the cavity enhanced spectroscopy. *Opto-Electron. Rev.*, 16(4), pp. 44-51

Wojtas, J., Bielecki, Z., Mikołajczyk, J. & Nowakowski, M. (2008). Signal processing system in portable NO_2 optoelectronic sensor, *Sensor+Test 2008 Proceedings*, Nurnberg, Germany pp. 105-108

Wojtas, J., Bielecki, Z., Stecewicz, T., Czyżewski, A., Mikołajczyk, J., Nowakowski, M. & Rutecka, B. (2009). Ultrasensitive NOx optoelectronic sensor. *Photonics Letters of Poland*, Vol. 1 (2), pp.85-87

Wojtas, J., Czyzewski, A., Stacewicz, T. & Bielecki, Z. (2006). Sensitive detection of NO_2 with Cavity Enhanced Spectroscopy, *Optica Applicata*, Vol. 36, No. 4, pp. 461-467

Wojtas, J., Czyżewski, A., Stacewicz, T., Bielecki, Z. & Mikolajczyk J. (2005). Cavity enhanced spectroscopy for NO2 detection, Proc. SPIE Vol. 5954, pp. 174-178

Ye, J., Ma, L.S. & Hall, J.L. (1997). Ultrasensitive high resolution laser spectroscopy and its application to optical frequency standards, *28th Annual Precise Time and Time Interval (PTTI) Applications and Planning meeting, Proceedings*, L. A. Breakiron, Ed., US Naval Observatory, Washington D.C., p. 289

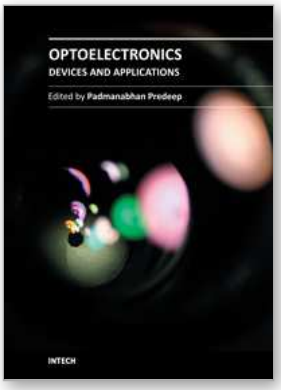

Optoelectronics - Devices and Applications

Edited by Prof. P. Predeep

ISBN 978-953-307-576-1
Hard cover, 630 pages
Publisher InTech
Published online 03, October, 2011
Published in print edition October, 2011

Optoelectronics - Devices and Applications is the second part of an edited anthology on the multifaced areas of optoelectronics by a selected group of authors including promising novices to experts in the field. Photonics and optoelectronics are making an impact multiple times as the semiconductor revolution made on the quality of our life. In telecommunication, entertainment devices, computational techniques, clean energy harvesting, medical instrumentation, materials and device characterization and scores of other areas of R&D the science of optics and electronics get coupled by fine technology advances to make incredibly large strides. The technology of light has advanced to a stage where disciplines sans boundaries are finding it indispensable. New design concepts are fast emerging and being tested and applications developed in an unimaginable pace and speed. The wide spectrum of topics related to optoelectronics and photonics presented here is sure to make this collection of essays extremely useful to students and other stake holders in the field such as researchers and device designers.

How to reference

In order to correctly reference this scholarly work, feel free to copy and paste the following:

Jacek Wojtas (2011). Detection of Optical Radiation in NOx Optoelectronic Sensors Employing Cavity Enhanced Absorption Spectroscopy, Optoelectronics - Devices and Applications, Prof. P. Predeep (Ed.), ISBN: 978-953-307-576-1, InTech, Available from: http://www.intechopen.com/books/optoelectronics-devices-and-applications/detection-of-optical-radiation-in-nox-optoelectronic-sensors-employing-cavity-enhanced-absorption-sp

INTECH
open science | open minds

InTech Europe
University Campus STeP Ri
Slavka Krautzeka 83/A
51000 Rijeka, Croatia
Phone: +385 (51) 770 447
Fax: +385 (51) 686 166
www.intechopen.com

InTech China
Unit 405, Office Block, Hotel Equatorial Shanghai
No.65, Yan An Road (West), Shanghai, 200040, China
中国上海市延安西路65号上海国际贵都大饭店办公楼405单元
Phone: +86-21-62489820
Fax: +86-21-62489821